ADVANCED OPTICAL MATERIALS

Supporting Information

for *Adv. Optical Mater.,* DOI: 10.1002/adom.202100230

Near-Infrared Active Metasurface for Dynamic Polarization Conversion

Pin Chieh Wu, Ruzan Sokhoyan, Ghazaleh Kafaie Shirmanesh, Wen-Hui Cheng, and Harry A. Atwater**

Near-Infrared Active Metasurface for Dynamic Polarization Conversion

Pin Chieh Wu[1,2], Ruzan Sokhoyan[2], Ghazaleh Kafaie Shirmanesh[2],

Wen-Hui Cheng[2], and Harry A. Atwater[2,3]

[1]Department of Photonics, National Cheng Kung University, Tainan 70101, Taiwan

[2]Thomas J. Watson Laboratory of Applied Physics, California Institute of Technology, Pasadena, California 91125, USA

[3]Kavli Nanoscience Institute, California Institute of Technology, Pasadena, California 91125, USA

Corresponding author: pcwu@gs.ncku.edu.tw; haa@caltech.edu

1. Active reflectance modulation with an Al metasurface

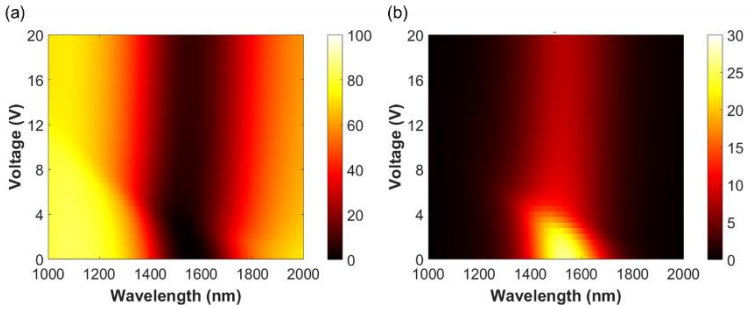

Figure S1. Simulated reflectance of the (a) co- and (b) cross-polarized light as a function of wavelength and applied voltage. The incident light is *y*-polarized. The structural dimensions are listed in the caption of Fig. 2.

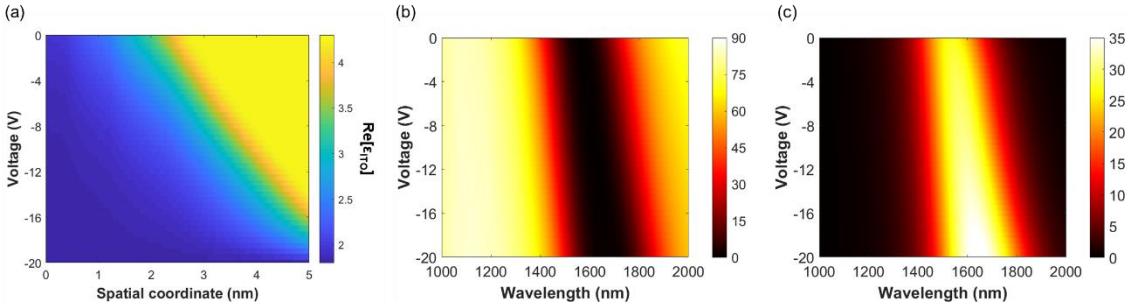

Figure S2. (a) Real part of the dielectric permittivity of the 5 nm-thick ITO layer Re[$\varepsilon_{\mathrm{ITO}}$] as a function of the spatial coordinate and applied voltage. In the considered Al/HAOL/ITO heterostructure, the spatial coordinate corresponds to the distance from the Al electrode so that the spatial coordinate of 5 nm corresponds to the ITO/HAOL interface. In (a), the wavelength is fixed to 1580 nm, the applied voltage is negative, indicating that (a) corresponds to the case of the reverse bias. (b) Simulated reflectance of the co- and (c) cross-polarized light as a function of wavelength and applied voltage in the case of the reverse bias. The incident light is *y*-polarized. The structural dimensions are listed in the caption of Fig. 2.

2. Tunable polarization conversion with an Al metasurface at different wavelengths

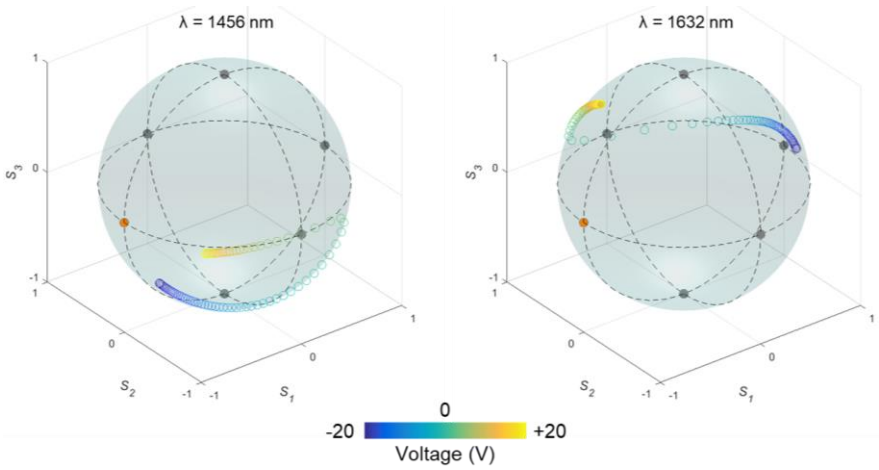

Figure S3. The voltage-dependent path of reflected light's polarization state on the Poincaré sphere at wavelengths of (left) 1456 nm and (right) 1632 nm. The incident light is *y*-polarized. The structural dimensions are listed in the caption of Fig. 2. The orange dot indicates the polarization state of the incident light.

3. Tunable polarization with Au metasurfaces

We developed an alternative design of the dynamic polarization converter based on a gate-tunable reflectarray metasurface with Au patch nanoantennas and an Au back reflector. Note that in the main text, we use Al nanoantennas and Al back reflector rather than Au. Our Au-based design consists of a 150 nm-thick Au back reflector, a 9.5 nm-thick HAOL gate dielectric, followed by a 5 nm-thick ITO layer, and an array of Au patch nanoantennas. The patch nanoantennas are 210 nm-long and 180 nm-wide (see Figure S4a). In case of the Au-based polarization converter, the nanoantennas' dimensions are slightly smaller as compared with the case of the Al-based polarization converter. The assumed thickness of the Au patch antennas is 140 nm. The period of the optimized metasurface is 350 nm for both *x*- and *y*-directions. The dielectric permittivity of ITO is described using the Drude model with constants $\varepsilon_\infty = 4.2345$, $\Gamma = 1.7588\times10^{14}$ (rad/s), $N = 2.8\times10^{20}$ (cm^{-3}), $m^* = 0.2525m_e$[1]. For the device physics simulation, the work function of Au is set to 5.1 eV. Figures S4b and S4c show the simulated reflectance spectra of co- and cross-polarized light, respectively. We observed significant reflectance modulation at telecommunication wavelengths for both co- and cross-polarization components when the electrical bias is applied. We observe strong reflectance modulation when the bias voltage is varied between 2 V and 4 V. The

observed active reflectance modulation indicates that we should be able to observe an active polarization control in the voltage range between 2 V and 4 V.

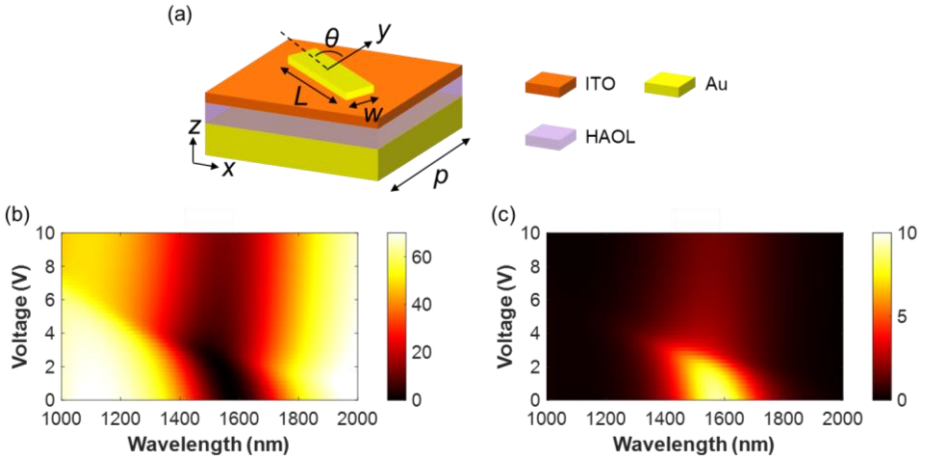

Figure S4. (a) Schematic of the tunable metasurface based on Au nanoantennas and Au back reflector. The metasurface consists of a 150 nm-thick Au back reflector, a 9.5 nm-thick HAOL layer, a 5 nm-thick ITO layer, and an array of 140 nm-thick Au patch antennas. The patch antenna dimensions are defined as L = 210 nm, w = 180 nm, and θ = 45°. The periodicity is p = 350 nm. Simulated reflectance of the (b) co- and (c) cross-polarized light as a function of wavelength and applied voltage. The incident light is y-polarized.

The phase difference between the two orthogonal polarization states (refer to as x- and y-components in this work) plays a key role in the polarization control. Figure S5a shows the phase difference between x- and y-components $\Delta\varphi = \varphi_{yy} - \varphi_{xy}$ as a function of the wavelength of the incident light and applied bias voltage. The white curve shows the condition when the x- and y-components of the reflected light have equal amplitudes. According to Figure S5a, a linear-to-circular polarization conversion can be realized at a wavelength of 1520 nm. Thus, in what follows, we will fix the wavelength to 1520 nm. Figure S5b plots the reflectance and the relative phase shift of x- and y-polarized components of the reflected light ($\Delta\varphi = \varphi_{yy} - \varphi_{xy}$) as a function of voltage at a wavelength of λ = 1520 nm. When the applied bias is about 2 V, a y-to-x polarization conversion is realized because the intensity of the y-polarized light is negligible in this voltage range. For the bias voltages of ~3V, the designed Au metasurface converts the incoming linearly polarized light into a circularly polarized light because of the 90° phase difference and equal reflectance of the x- and y-polarized light. For the other voltages, our metasurface realizes a linear-to-elliptical polarization conversion. Figure S5c plots Stokes parameters as function of wavelength and applied voltage. Similar to what we observed in the Al-based tunable polarization converter, the S_1 exhibits a

significant change when the applied electrical bias crosses a particular value (~2.5V in this case). This is consistent with the result of the amplitude modulation in which a significant change can be observed when the electrical bias crosses the voltage value of ~2.5 V. The parameter S_3 also shows a dramatic change and reaches about +1 at this voltage value, revealing the possibility of the circular polarization conversion. As compared to the Al-based metasurface, this Au metasurface requires much lower gate voltage to achieve linear-to-circular polarization conversion that significantly facilitates the experimental demonstration. Next, we plan to experimentally demonstrate this Au-based polarization converter.

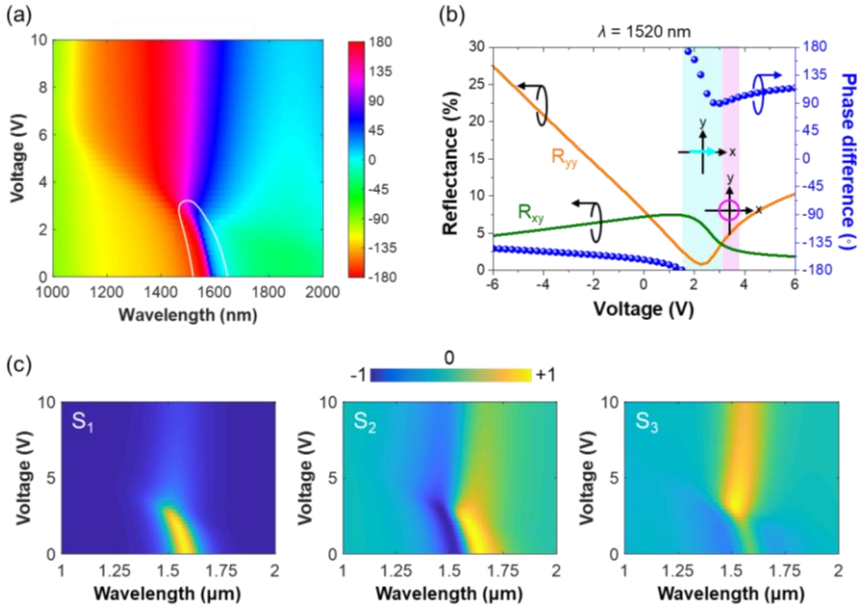

Figure S5. (a) Phase difference between *x*- and *y*-components as a function of wavelength and applied bias. The white solid line marks the parameter values that yield equal reflectance values for *x*- and *y*-polarized components of light. (b) Simulated reflectance (orange line: cross-polarized light; olive line: co-polarized light) and phase difference (phase of the cross-polarized reflected wave minus the phase of the co-polarized reflected wave) as a function of applied bias. The metasurface is illuminated by a *y*-polarized normally incident light. The cyan and magenta shadowed regions indicate the voltage range where desired polarization states are obtained. The operation wavelength is 1520 nm. (c) Plot of the Stokes parameters versus applied electrical bias.

To experimentally evaluate the performance of the proposed metasurface polarization converter, we have fabricated the described Au metasurface-based active polarization converter.

For sample preparation, we first patterned some alignment markers using electron beam lithography [VISTEC electron beam pattern generator (EBPG) 5000+] at an acceleration voltage of 100 keV and with a current of 50 nA. Then the bottom contact (150-nm-thick Au with an adhesion layer of 5-nm-thick Ti) is fabricated. Subsequently, a gate dielectric HAOL is deposited through a shadow mask by using a thermal recipe in the ALD tool (Fiji G2 Plasma Enhanced Atomic Layer Deposition System) at 150°C using the recipe described in Ref [2]. The thickness of the HAOL film was measured by transmission electron microscopy (TEM). Figure S6 shows the TEM image of the HAOL film deposited on a Si substrate. According to the TEM image, the thickness of the deposited HAOL layer is very close to what we numerically designed. Once the area of HAOL is determined, the ITO layer is subsequently defined by electron beam lithography with alignment markers and deposited using room-temperature RF magnetron sputtering in an Ar/O_2 plasma environment. The deposition pressure and the applied RF power were set to 3 mTorr and 48 W, respectively. The plasma was struck by using argon (Ar) gas with a flow rate of 20 sccm. A mixture of argon and oxygen (O_2) gases (Ar/O_2: 90/10) was used to control the amount of oxygen deficiency, and hence, the charge carrier concentration of the ITO layer. We characterized the ITO layer by a combination of Hall measurements and spectroscopic ellipsometry on the ITO films deposited on quartz and Si substrates, respectively[2]. The fitted thickness of the ITO layer obtained through the ellipsometry measurement was 4.8 nm. Finally, the metasurface block along with the top contacts are patterned with the fourth electron beam writing process at an acceleration voltage of 100 keV with a beam current of 300 pA.

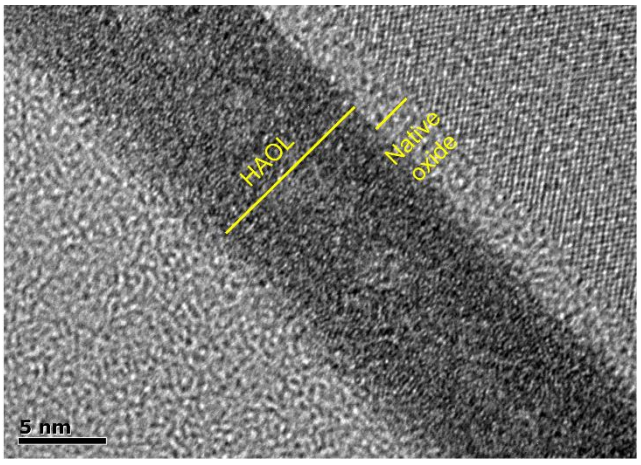

Figure S6. TEM image of the HAOL control sample deposited on a Si substrate *via* ALD.

Figures S7a and S7b show the schematic of the proposed device and the SEM image of the fabricated Au metasurface, respectively. To optically characterize the polarization state of reflected light, a quarter-wave plate paired with a linear polarizer is inserted in front of the spectrometer, as shown in Figure S7c. A visible camera is utilized to visualize the position where the spectrometer will measure. Figure S7d shows the measured reflectance as a function of wavelength and voltage for six polarization states when the incoming light is *y*-polarized. As expected, we observed a resonant dip in the LP-V spectrum associated with a polarization conversion peak in the LP-H spectrum when the electrical bias is absent. When the electrical bias is increased from 0 V to +10 V, we can see that the intensity of the cross-polarized light slightly increased at a wavelength of ~1.5 μm, then saturated at ~60% when the applied bias is greater than a certain level. Interestingly, the reflectance in the LP-H spectrum shows a significant decrease when the bias voltage is changed from 0 V to -4 V. Similar intensity variation can be observed for the cases of RCP, and LP+45˚. We also found that the resonant features in RCP and LP+45˚ spectra become narrower when the electrical bias region varied from negative to positive, while the LP-H spectrum becomes broader. Contrarily, for the cases of LP-V, LCP, and LP-45˚, the reflectance spectrum shows slight changes when bias voltage is varied. Based on these results, we conclude that when illuminated by the linearly polarized light, the metasurface can dynamically control the polarization state of the reflected light.

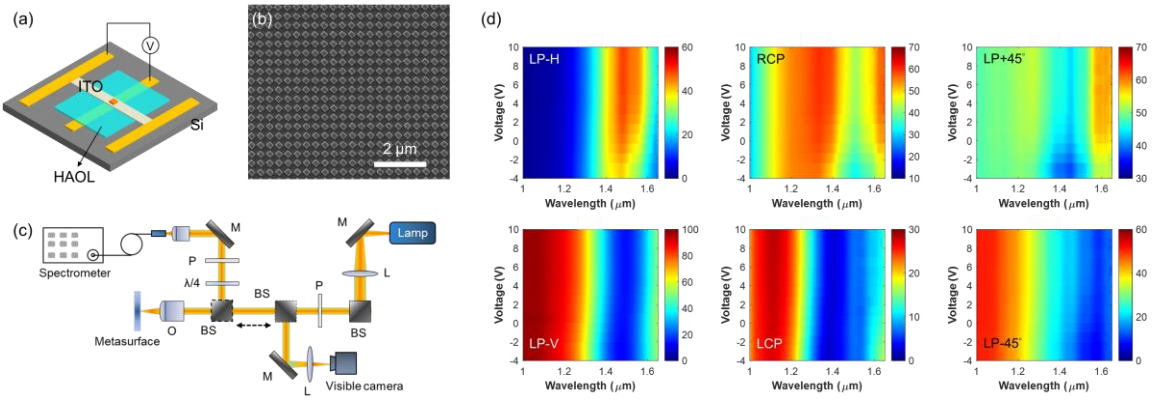

Figure S7. (a) Schematic illustration of the tunable polarization converter sample based on Au metasurface. (b) Scanning electron microscopy image of the fabricated sample. The beam splitter with dashed-boundary is moved back and forth for either visualizing the sample surface or measuring spectral signal. (c) Schematic for the measurement optical setup. M: mirror, L: lens, BS: beam splitter, λ/4: quarter-wave plate, P: linear polarizer, O: objective. (d) Experimental spectra for different polarization states of reflected beam under different applied biases. The legend of LP-H, LP-V, RCP, LCP, LP+45˚, and LP-45˚ correspond to *x*-

polarization, *y*-polarization, right-hand circular polarization, left-hand circular polarization, linear polarization along +45˚, and linear polarization along -45˚, respectively.

To clearly distinguish the generated polarization state of the reflected light, we calculate the Stokes parameters using the results from Figure S7d. Figure S8 shows the measured Stokes parameters. The parameters S_1, S_2, and S_3 are normalized to S_0 so that the parameter values vary between -1 and +1. We experimentally observe that both S_2 and S_3 are electrically modulated at a wavelength of ~1.5 μm. Although the measurement results show that the fabricated metasurface can electrically modulate the Stokes parameters, the intensity variations are less significant as compared with our theoretical predictions (cf. Figure S5c). The general trends observed in measurements are quite different from those obtained in simulations. Besides, we haven't been able to experimentally identify the situation where S_3 is unity and $S_1 = S_2 = 0$, which implies that we haven't been able to experimentally achieve liner-to-circular polarization conversion. This difference actually arose from the mismatch between the ITO Drude parameters used in simulations and the ones in the real sample.

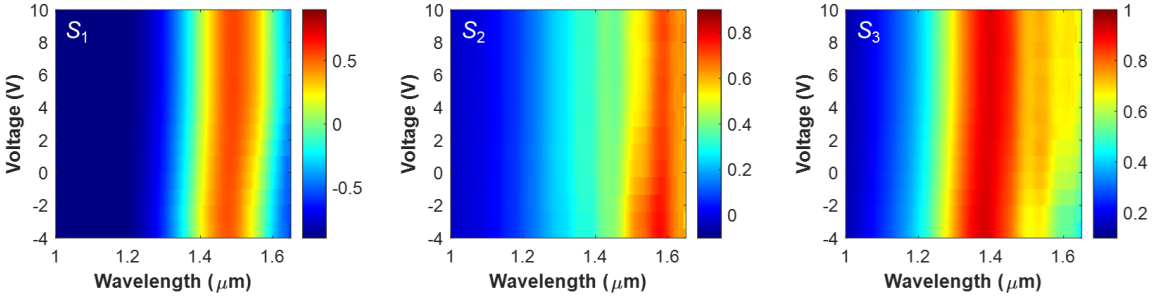

Figure S8. Experimentally measured Stokes parameters versus incident wavelength and applied electrical bias.

Based on our recent works in which we have experimentally characterized the optical properties of the ITO film[2, 3], the parameters of the deposited ITO can are given by the following Drude parameters: $\varepsilon_\infty = 3.9$, $\Gamma = 1.8\times10^{14}$ (rad/s), $N = 3\times10^{20}$ (cm^{-3}), $m^* = 0.35m_e$. But the Drude parameters used in the design of the tunable polarization converter are based on the values obtained in our earlier work[1]. Next, we assess how the variation of the Drude parameters affects the optical performance of our tunable polarizer. We fix the geometrical parameters of our metasurface to those defined in Figure S4a and change the Drude parameters of the ITO layer, adopting the values reported in our recent work[3]. Figure S9 plots the simulated Stokes parameters. When comparing

Fig. S8 and Fig. S9 we observe that our experimental and simulation results qualitatively match. Please notice that here we also revise our device physics simulations according to the modified Drude parameters. For example, the effective electron mass of ITO is now taken as $m^* = 0.35m_e$. Similarly, we can see all three Stokes parameters exhibit much weaker modulation as compared with simulation results shown in Figure S5c, indicating that the accurate determination of the Drude parameters of ITO is crucial for obtaining the optimized performance of the tunable polarization converter.

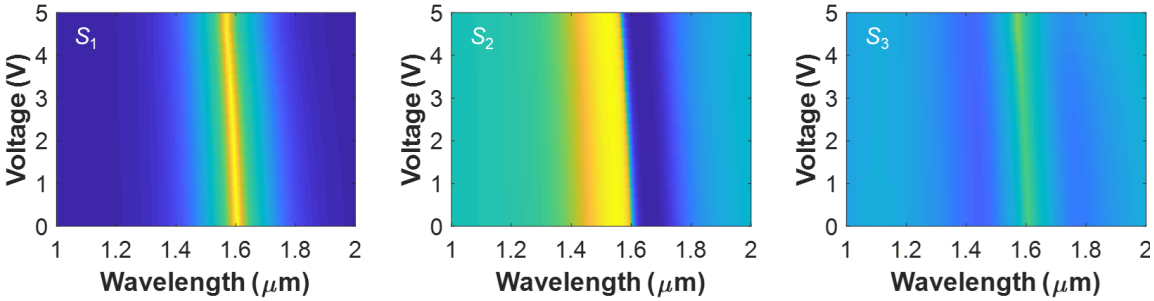

Figure S9. Simulated Stokes parameters as a function of wavelength applied electrical bias. The structural parameters of Au metasurface are from Fig. S4a, and the Drude model parameters of ITO are from Ref. [3].

Next, we assume that the Drude parameters of the ITO layer are given in Ref. [2, 3] and optimize the structural dimensions of the Au metasurface-based tunable polarization converter. The geometrical motif of the metasurface is the same as the one shown in Figure S4a. Figure S10 shows the simulated results after structural optimization. The metasurface consists of a 150-nm-thick Au back reflector, a 15-nm-thick HAOL, a 5-nm-thick ITO, and an array of 100 nm-thick Au patch antennas. The dimensions of the metasurface unit cell are given as L = 210 nm, w = 180 nm, θ = 45°, and p = 350 nm. First, we evaluate the reflectance modulation capability of the designed metasurface before characterizing its polarization conversion performance. As shown in Figures S10a and S10b, when the electric bias is 0 V, a strong linear cross polarization conversion effect can be observed around the telecom wavelengths. The highest cross polarization conversion efficiency is ~15%, which is higher than what we observed in the previous design. When the electrical bias is increased up to ~4 V, the conversion peak firstly blue-shifts and then red-shifts when the bias voltage is further increased. Overall, the spectral features are very similar to the results shown in Figures S4 and S5, indicating that we are able to control the polarization of the reflected light when applying electrical bias.

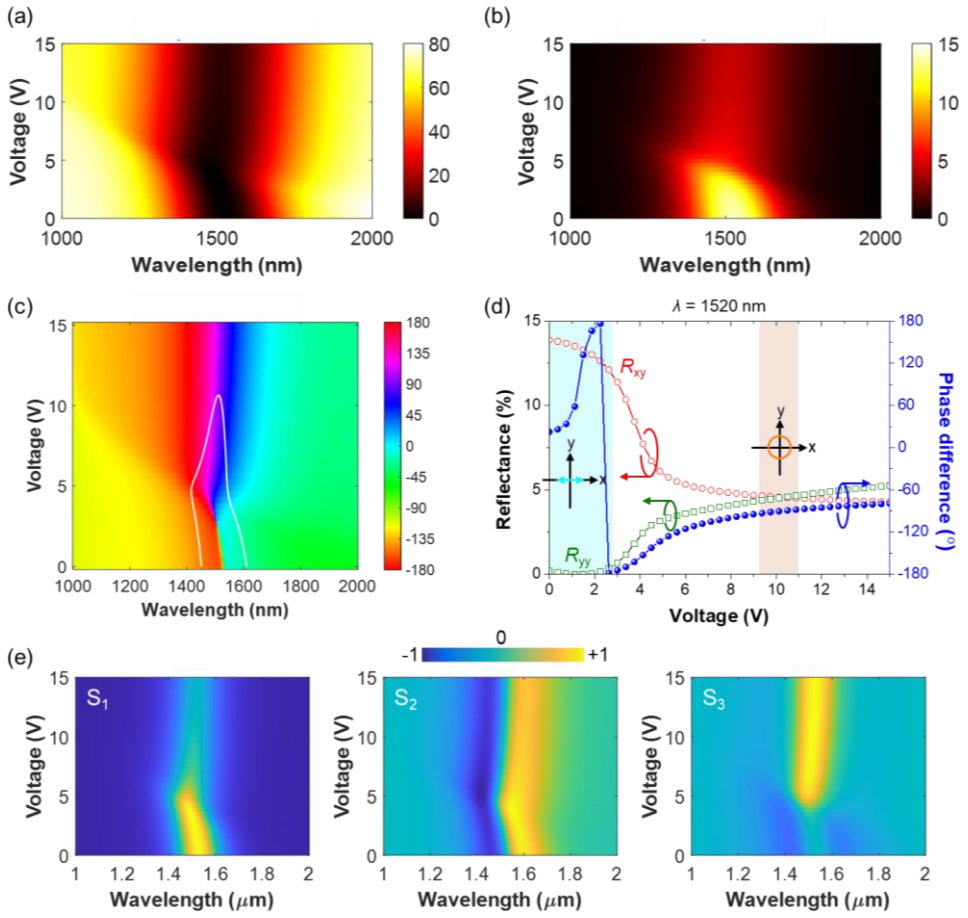

Figure S10. Simulated reflectance of the (a) co- and (b) cross-polarized light as a function of wavelength and applied voltage. The incident light is *y*-polarized. The metasurface consists of a 150-nm-thick Au back reflector, a 15-nm-thick HAOL layer, a 5-nm-thick ITO layer, and an array of 100 nm-thick Au patch antennas. The geometrical parameters of our unit cell are given as: L = 210 nm, w = 180 nm, and θ = 45°. The metasurface period is p = 350 nm. (c) Phase difference between *x*- and *y*-components as a function of wavelength and applied bias. The white solid line marks the parameter values that yield equal reflectance values for *x*- and *y*-polarized components of light. (d) Simulated reflectance (red line: cross-polarized light; olive line: co-polarized light) and phase difference (phase of the cross-polarized reflected wave minus the phase of the co-polarized reflected wave) as a function of applied bias. The metasurface is illuminated by a *y*-polarized normally incident light. The cyan and orange shadows indicate the range of voltage values where desired polarization states are obtained. The operating wavelength is 1520 nm. (e) Stokes parameters as a function of wavelength and applied electrical bias.

To identify the optimal wavelength for linear-to-circular polarization conversion, we investigate the phase difference between *x*- and *y*-polarized components of the reflected light. In Fig. S10c, the solid line labels the condition where the *x*- and *y*-polarized components yield equal reflectance (see Figure S10c). Our analysis shows that we can obtain three polarization states at a wavelength of 1520 nm. The active polarization conversion performance is summarized in Figure S9d. Again, three polarization states are successfully realized when the electrical bias is applied in an appropriate voltage range:

$0\ \text{V} \leq V_a \leq 2.8\ \text{V}$ – linear to cross-polarized linear polarization conversion,

$9.2\ \text{V} \leq V_a \leq 11.1\ \text{V}$ – linear-to-circular polarization conversion,

Other voltage values – linear-to-elliptical polarization conversion,

where V_a is the applied electrical bias. The simulated Stokes parameters exhibit very similar trends to the previously discussed cases (Figure 5b in the main article and Figure S5c): S_1 and S_3 vary significantly when the applied bias goes across ~5 V. When the condition $S_1 = S_2 = 0$ ($S_2 = S_3 = 0$) and $S_3 = 1$ ($S_1 = 1$) holds linear-to-circular (*y*-to-*x* cross) polarization conversion occurs. Moreover, we found that structural dimensions of our redesigned metasurface are quite close to our orginal Au-based metasurface design. When comparing our original Au metasurface-based design and the redesigned polarization converter, we observe that only the thicknesses of the Au patch antenna and the HAOL layer are slightly changed if the ITO parameters shifted, indicating that the proposed design motif is quite robust.

4. Linear cross-polarization conversion for different thicknesses of Al nanoantennas

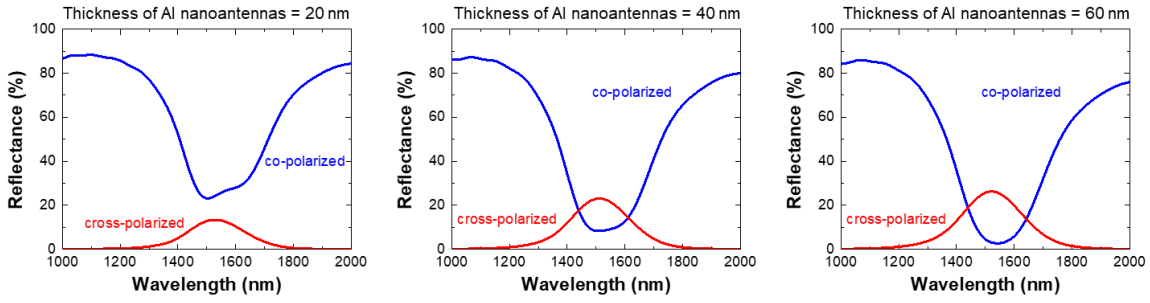

Figure S11. Simulated co-polarized (blue lines) and cross-polarized (red lines) reflectance spectra of the tunable metasurface for different thicknesses of Al nanoantennas. The co-polarized reflectance shows a non-zero intensity at a wavelength of 1580 nm when the thickness of Al nanoantennas is less than 80 nm. Thus, to realize a complete conversion to a linear cross-polarized state and to minimize the fabrication difficulty

during the lift-off process , we choose the Al nanoantenna thickness as 80 nm. The co-polarized and cross-polarized reflectance spectra for metasurfaces with 80-nm-think Al nanoantennas can be found in Fig. 3a.

5. Linear cross-polarization conversion performance for different polarization angle of incident light

As discussed in the main article, the polarization conversion is achieved by simultaneously exciting two gap plasmon modes that are supported by the long side and short side of the Al nanoantenna, respectively. Thus, a nonideal incident polarization angle can influecne the polarization conversion performance. In this section, we briefly discuss the effect of the misalignment between the incident polarization angle and the Al nanoantenna orientation on the polarization conversion performance. For simplicity, the applied bias is set to 0 V. Figure S12a shows the simulated x-component (blue dots) and y-component (navy blue dots) reflectance spectra as a function of polarization angle θ_{pol}. At no applied bias we expect to obtain an x-polarized reflected light of high purity. Therefore, when ananlysing the the polarization characteristics of the refelcted light, we expect that the intensity of the x-component has to be significantly higher than the intensity of the y-component. To quantitatively analyze the linear cross-polarization conversion performance, we utilize a figure of merit named the intensity ratio, which is defined as a ratio of the reflectance intensity of the y-component and the reflectance intensity of the x-component. As seen in Fig. S12a (red circles), the intensity ratio acqures relatively low values when the polarization angle is around 0°. We observe that the intensity ratio is less than 0.05 when the polarization angle is varied between 5° and 10°, indicating that a highly pure x-polarized light is obtained in reflection. The intensity ratio increases very significantly when the polarization angle is far away from 0°. The intensity ratio even reaches unity when the polariztion angle equals to 45° or -45°. This is because only one single plasmon mode is excited under such conditions, leading to a linearly-polarized reflected light along either 45° or -45°. To further evaluate the polarization conversion performance, we plot the polarization angle-dependent path of the polarization states on the Poincaré sphere. As expected, a nearly ideal x-polarized light can be realized when the polarization angle is close to 0°. The polarization state of the reflected light deviates from the target one when the polarization angle increases. As seein in Fig. S12(b), the reflected light becomes linearly polarized light along 45° and -45° when the polarization angle is 45° or -45°, respectively. In summary, to avoid a siginificant deviation of the resulting polarization state of the reflected light from the target one, the polariztion angle of incident light has to be within <5°.

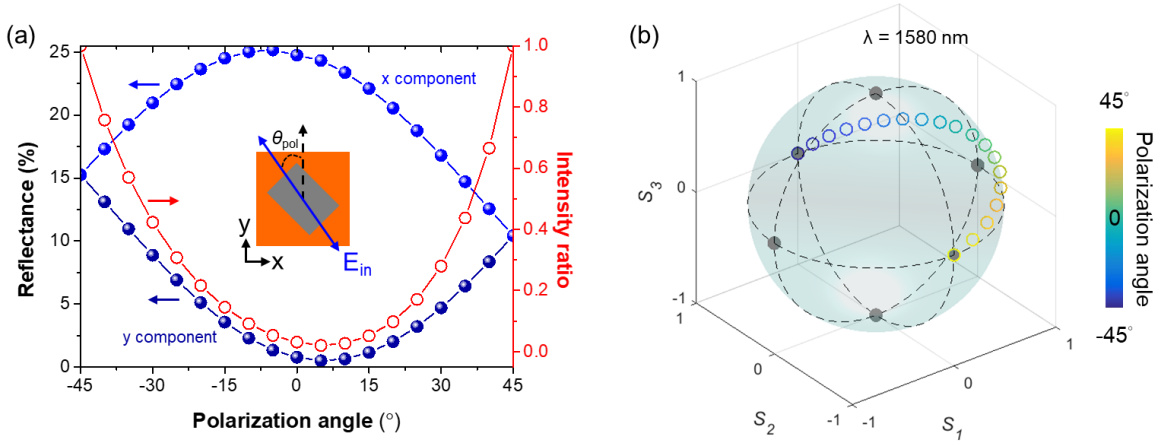

Figure S12. (a) Simulated reflectance of the x-component (blue dots) and y-component (navy blue dots) as a function of incident polarization angle θ_{pol} for the Al tunable metasurface at 0 V. The red circles show the ratio of the reflectance of the y-polarized and x-polarized light. The inset shows the orientation of the Al patch nanoantenna with respect to the *y*-axis. The incident polarization is aligned to the long axis(short axis) of the Al nanoantenna when the polarization angle θ_{pol} = 45° (-45°). (b) The polarization angle-dependent path of the polarization state of the reflected light on the Poincaré sphere. Incident wavelength: 1580 nm.

Reference

[1] Y.-W. Huang, H. W. H. Lee, R. Sokhoyan, R. A. Pala, K. Thyagarajan, S. Han, D. P. Tsai, H. A. Atwater, *Nano Lett.* **2016**, 16, 5319.

[2] G. Kafaie Shirmanesh, R. Sokhoyan, R. A. Pala, H. A. Atwater, *Nano Lett.* **2018**, 18, 2957.

[3] G. K. Shirmanesh, R. Sokhoyan, P. C. Wu, H. A. Atwater, *ACS Nano* **2020**, 14, 6912.